Crystal structure of A-type ATP synthase catalytic nucleotide-binding subunit A from *Pyrococcus horikoshii* reveals a novel domain related in the peripheral stalk

Yuki Maegawa, Hazuki Morita, Daisuke Iyaguchi, Min Yao, Nobuhisa Watanabe* and Isao Tanaka

Division of Biological Sciences, Graduate School of Science, Hokkaido University, Japan. E-mail: nobuhisa@sci.hokudai.ac.jp

Synopsis The first X-ray structure of the catalytic nucleotide-binding subunit A of the A_1-ATPase has been determined at 2.55 Å resolution.

Abstract H^+-transporting ATP synthase is a multi-subunit enzyme involved in the production of ATP, which is essential molecule for living organisms as a source of energy. Archaeal A-type ATPase (A-ATPase) is thought to act as a functional ATP synthase in Archaea and is thought to have chimeric properties of F-ATPase and V-ATPase. From the previous structural studies of F-ATPase, it is indicated that the major nucleotide-binding subunits α and β consist of three domains. The catalytic nucleotide-binding subunit A of V/A-ATPase contains an insertion of about 90 residues, which is absent from the F_1-β subunit. Here we describe the first X-ray structure of the catalytic nucleotide-binding subunit A of the A_1-ATPase determined at 2.55 Å resolution. A_1-ATPase subunit A from *Pyrococcus horikoshii* consists of four domains. A novel domain, including a part of this insertion, corresponds to the "knob-like structure" observed in electron microscopy of A_1-ATPase. Based on the structure, it is highly likely that this inserted domain is related to the peripheral stalk common to the A- and V-ATPases. The arrangement of this inserted domain suggests that this region plays an important role in A-ATPase as well as in V-ATPase.

Keywords: H^+-transporting ATP synthase; A-ATPase; catalytic nucleotide-binding subunit A; archaea; X-ray crystallography

1. Introduction

H^+-transporting ATP synthase (H^+-ATPase; EC 3.6.3.14) is a multi-subunit enzyme involved in the production of ATP. F-type ATPase (F-ATPase) acts as a functional ATP synthase in rotational mode driven by a proton electrochemical potential gradient (Yasuda *et al.*, 2001). The vacuolar-type ATPase in vacuoles and clathrin-coated vesicles (V-ATPase) pumps H^+ rather than synthesizing ATP under physiological conditions, although its structure is similar to that of the F-type enzyme (Forgac, 1999; Futai *et al.*, 1998). Archaeal A-type ATPase (A-ATPase) is the third class belonging to the H^+-translocating ATPase superfamily (Schafer & Meyering-Vos, 1992) and is thought to have chimeric properties of F-ATPase and V-ATPase with regard to structure and function (Becher & Muller, 1994;

Mukohata & Yoshida, 1987; Ihara & Mukohata, 1991; Hochstein, 1992; Dirmeier *et al.*, 2000; Wilms *et al.*, 1996). Each enzyme in the three classes mentioned above consists of two sectors: a hydrophilic catalytic headpiece sector ($F_1/V_1/A_1$) and a membrane sector ($F_O/V_O/A_O$) (Fig. 1A). The catalytic headpiece sectors (containing the $\alpha_3\beta_3$ subcomplex in F_1, A_3B_3 in V_1/A_1) are connected *via* the F_1-γ subunit or the V_1/A_1-D subunit to the membrane sectors. The major nucleotide-binding subunits in F_1-ATPase are catalytic β and non-catalytic α, whereas the corresponding subunits in V_1/A_1 are catalytic A and non-catalytic B. Previous structural studies indicated that F_1-α and β subunits consist of three domains: the N-terminal domain, nucleotide-binding domain, and C-terminal domain (Abrahams *et al.*, 1994; Leyva *et al.*, 2003). However, the catalytic subunit A of V_1/A_1 contains an insertion of about 90 residues called the non-homologous region (NHR), which is highly conserved among A subunits but is absent from the F_1-β subunit, between the N-terminal and nucleotide-binding domains (Zimniak *et al.*, 1988; Bowman *et al.*, 1988; Hirata *et al.*, 1990; Puopolo *et al.*, 1991). The results of mutational analysis of this region of *Saccharomyces cerevisiae* (*Sce*) V_1-A subunit suggested that NHR is likely to form a unique domain and form part of a peripheral stalk connection between the V_1 and V_O domains (Shao *et al.*, 2003; Shao & Forgac, 2004). Moreover, recently reported structures of the A_1 headpiece and A_1A_O by electron microscopy revealed the existence of a knob-like structure in the catalytic subunit A, which is not found in the F_1 headpiece (Coskun, Radermacher *et al.*, 2004; Coskun, Chaban *et al.*, 2004).

Here, we report the first X-ray structure of the catalytic nucleotide-binding subunit A of the A_1-ATPase at 2.55 Å resolution.

2. Materials and Methods

2.1. Crystallization and data collection

Pyrococcus horikoshii (*Pho*) ATPase subunit A was expressed, purified, and crystallized in a form corresponding to the product of intein-mediated protein splicing as described previously (Maegawa *et al.*, 2004). Crystals of selenomethionine (Se-Met)-substituted A subunit were also prepared for MAD phasing. In the case of Se-Met-substituted A subunit, cells were grown at 37 °C in M9 minimal medium supplemented with 25 μg mL^{-1} Se-Met in place of methionine, 50 μg mL^{-1} ampicillin, and thiamine. At an OD_{600} of 0.6, the cells were induced by addition of 1 mM IPTG and growth continued at 37 °C for 17 h. Subsequent steps were the same as described and crystals of the Se-Met-substituted A subunit were obtained under the same conditions as the native protein (Maegawa *et al.*, 2004).

All X-ray diffraction experiments were performed at -173 °C, with crystals cooled in a nitrogen gas stream. Crystallization solution (46 - 50% (*v*/*v*) MPD) was also used as cryoprotective solution. The native dataset was collected at beamline BL41XU of SPring-8, and a complete MAD dataset from a single crystal of Se-Met-incorporated A subunit was collected at beamline BL18B of Photon Factory. Data collection statistics are summarized in Table 1.

2.2. Structure determination and crystallographic refinement

Eleven of eighteen expected Se sites in the asymmetric unit were found by SOLVE (Terwilliger, 2004), and were further refined using SHARP (Fortelle & Bricogne, 1997). Finally, seventeen Se sites were found and used to phase the structure factor by SHARP. The electron densities were improved by solvent-flattening with SOLOMON (Abrahams & Leslie, 1996). Density modification was performed with ARP/wARP (Morris *et al.*, 2003) and DM (Cowtan, 1994) in the CCP4 program package (Collaborative Computational Project, 1994). The initial model of subunit A was built manually using the program O (Jones *et al.*, 1991). Crystal averaging between the native and Se-Met crystals using DMMULTI (Cowtan, 1994) in the CCP4 program package (Collaborative Computational Project, 1994) was performed to improve the map quality. After construction of the molecular model for residues 59–588, side chains were generated automatically using ARP/wARP (Morris *et al.*, 2003). Several cycles of manual fitting with O combined with refinement by conjugate gradient minimization and B-factor refinement with CNS (Brunger *et al.*, 1998) were carried out. The final refined model included 549 amino acid residues and one MPD molecule. Residues 1–59 and 341–356 were unidentified in the electron density map, and thus molecular models for these segments are not present in the final model. As the side chains of residues 60–66 were also unidentified in the electron density map, the main chains of these segments were constructed as poly-glycine chains in the final model. The crystallographic R factor for reflections between 10.0–2.55 Å resolution was 23.9% with a free R factor of 27.1% based on the subset of 10% of the reflections. The statistics for phasing and refinement are also summarized in Table I. Atomic coordinates of the A subunit of *Pho* A-ATPase have been deposited in the PDB as entry 1VDZ.

3. Results and Discussion

Catalytic nucleotide-binding subunit A has a warped cylindrical structure with approximate dimension of 55 Å × 55 Å × 100 Å (Fig. 1B). This subunit consists of four domains: Domain I (N-terminal domain, residues 1-79, 110-116, 189-199), Domain II (corresponds to the "knob-like structure" observed in electron microscopy (Coskun, Radermacher *et al.*, 2004; Coskun, Chaban *et al.*, 2004), residues 117-188), Domain III (nucleotide-binding domain, residues 80-99, 200-437), and Domain IV (C-terminal domain, residues 438-588). Based on the amino acid sequence alignment, the N-terminal disordered region (Met 1 to Val 59) and Arg 60–Leu 76 are likely to correspond to the N-terminal crown region consisting of seven β-strands in the N-terminal domain of F_1-α and β subunits (Abrahams *et al.*, 1994). Loose crystal packing due to fact that A subunit was not crystallized in complex with other subunits such as B and D as well as high solvent content (61.2%) may have caused flexibility in most of the N-terminal domain and some parts of the nucleotide-binding domain, and thus cause these regions to be disordered or to have high B-factor. With the exception of Domain II protruding toward the outside of this subunit, the overall structure of subunit A closely resembles those of F_1-ATPase catalytic subunit β and non-catalytic subunit α, despite the low levels of sequence identity (about 20%, Fig. 1C).

In the major nucleotide-binding subunits, α and β of F_1 and A and B of A_1/V_1, two nucleotide-binding motifs, Walker A motif (also called nucleotide binding P-loop, GPFGSGKT, residues 234–241), and Walker B motif (RDMGYDDVALMAD, residues 320–331), are conserved (Walker *et al.*, 1982). All the residues that are essential for nucleotide-binding and enzyme activity in the β subunit of the F_1-ATPase are strictly conserved in the primary sequence of A subunit of both the A- and V-ATPase (Fig. 2A). No electron density corresponding to ATP, ADP, or Mg^{2+} was observed in the nucleotide-binding site. The geometry of the active site is essentially the same as the F_1-β subunit. This conservation of the active site geometry in the catalytic subunit A of A-ATPase strongly suggests that A-ATPase employs the same mechanism as F-ATPase.

The DELSEED sequence in the C-terminal domain of the bovine mitochondria F_1-β subunit, which moves and contacts the rotor γ subunit when the nucleotide fills the catalytic site (Hara *et al.*, 2000; Hara *et al.*, 2001), is substituted for DALPERE (residues 482–488) in *Pho* A_1-ATPase A subunit (Fig. 2B). Bovine F_1-βDELSEED motif has five acidic residues, whereas this region of *Pho* A_1-A subunit has only three acidic residues. Negative charges in the F_1-βDELSEED motif do not play a direct role in torque generation but the acidic property plays a role in the inhibitory effect by the intrinsic inhibitor, F_1-ε subunit (Hara *et al.*, 2000; Hara *et al.*, 2001). The residues related to the interaction between A and D/F subunits of A-ATPase have not been determined precisely, but catalytic subunit A is likely to connect with D and/or F subunit *via* this region. Further studies from both biochemical and structural perspectives are required to elucidate the role of this region in rotation catalysis of the A-ATPase.

Domain II, the novel domain which corresponds to the knob-like structure in the electron microscopy projection of A_1A_O ATP synthase (Coskun, Radermacher *et al.*, 2004; Coskun, Chaban *et al.*, 2004), was revealed between Domain I (N-terminal domain) and Domain III (nucleotide-binding domain). According to the model of subunit topology in the A_1A_O complex proposed based on biochemical and structural data (Coskun, Radermacher *et al.*, 2004; Coskun, Chaban *et al.*, 2004), Domain II protrudes toward the opposite side of the central rotor (Fig. 1A and 1B). Domain II is a peripheral domain including a part of NHR, which is about 90 amino acids and is highly conserved between A- and V- ATPase catalytic nucleotide-binding subunit A but absent in the F-ATPase (Pro122–Pro210 of *Pho* A_1-A subunit, Fig. 2C). The structure-based sequence alignment provided detailed information on this region. NHR previously assigned for *Sce* is not fully corresponds with Domain II of *Pho* A_1-A subunit. Actually, C-terminal region of the previously assigned NHR, Met189–Pro210 of *Pho* A_1-A subunit and Thr114–Ile136 of bovine F_1-β subunit are homologous. Furthermore, Lys117-Ile121 of Domain II of *Pho* A_1-A subunit has no homologous reagion to F_1-β. The structure of *Pho* A_1-A subunit suggests that we should modify the assignment of NHR as Lys117-Lys188.

Domain II of *Pho* A_1-A subunit is a peculiar domain comprised of eight β-strands and is folded into a compact β-sandwich structure with internal twofold symmetry (Fig. 1D). The fold of this domain is very similar to the crystal structure of the biotinyl/lipoyl domain (Fig. 1E), for example, biotinyl domain of acetyl-CoA carboxylase (PDB: 1BDO) (Athappilly & Hendrickson, 1995) and the solution structures of biotin carboxyl carrier domain of transcarboxylase (PDB: 1DCZ) (Reddy *et al.*, 2000), the lipoyl domain of pyruvate dehydrogenase (PDB: 1IYU,

1QJO) (Berg *et al.*, 1997; Jones *et al.*, 2000), and the lipoyl domain of 2-oxoglutarate dehydrogenase (PDB: 1GHJ) (Berg *et al.*, 1996). Despite the low levels of sequence identity (14–25%), superposition of the backbone of Domain II onto these domains gives rms values of 0.9–1.4 Å. However, comparison between Domain II of *Pho* A_1-A subunit and the domains of other proteins indicates two differences: absence of a Lys residue to be biotinylated or lipoylated, and the topology of the strands. First, the target of biotinylation or lipoylation is the Lys residue located in the loop between the fourth and fifth strands, whereas the residue at this position is Ser143 in *Pho* A_1-A subunit. Second, although seven strands are compatible in both length and location, the last strand in Domain II (residues 184–187) corresponds to the first strands in the other domains, resulting in a difference in the topology.

Sce NHR has been reported to bind directly to the V_O domain, and mutation in NHR causes a change in proton transport or ATPase activity and defective assembly of V-ATPase (Shao *et al.*, 2003; Shao & Forgac, 2004). The peripheral location of Domain II of *Pho* A_1-A subunit implies that this domain forms part of the peripheral stalk connecting A_1 and A_O domains. Taking the results of mutational analysis of *Sce* NHR of V_1-A subunit into account (Shao *et al.*, 2003; Shao & Forgac, 2004), it is highly likely that Domain II in the A subunit is related to the peripheral stalk common to the A- and V-ATPases. Although the detailed effects of mutation of the residues in Domain II or NHR have not been reported in A-ATPase, it is reasonable to suggest that this region plays an important role in A-ATPase as well as in V-ATPase based on the similarities in sequence, composition, and topology of the subunits. Further investigations, including structural analysis of the A-ATPase complex or structural analysis of Domain II in complex with the subunits forming part of the peripheral stalk of A-ATPase will be necessary to determine whether this domain actually contributes to the peripheral stalk connecting A_1 and A_O.

Figure 1 Catalytic nucleotide-binding subunit A of *Pho* A-ATPase. (A) Schematic model based on the model of *Methanococcus janashii* A-ATPase (Coskun, Chaban *et al.*, 2004). Three catalytic A subunits are colored gray. (B) Structure of *Pho* A-ATPase catalytic nucleotide-binding subunit A. (C) Overall structure of the catalytic nucleotide-binding subunit β of bovine mitochondrial F-ATPase (empty form). (D) Domain II. The direction of view is approximately horizontal to that in (B). Eight β strands are represented as S1–S8, respectively. (E) Archetype of the similar structures of Domain II, biotinyl domain of acetyl-CoA carboxylase (PDB: 1BDO). Biotynylated lysine residue is represented as a ball-and-stick model.

Figure 2 Amino acid sequence comparison of A/V/F-ATPase catalytic nucleotide-binding subunits. Pho: *Pho* A_1-A subunit, Sce: *Sce* V_1-A subunit, BM: bovine mitochondrial F_1-β subunit. (A) The nucleotide-binding site. Only residues corresponding to Gly234–Glu267 in *Pho* A_1-A subunit are shown. Residues conserved in the catalytic nucleotide-binding subunits are shown in blue. Residues identical in *Pho* and *Sce* are shown in light blue. The sequence highlighted in the box corresponds to the nucleotide-binding P-loop. Nucleotide-binding residues are shown in red. (B) Comparison around DALPERE sequence (residues 482–488) corresponding to F_1-βDELSEED. Residues conserved in the catalytic nucleotide-binding subunits are shown in blue. Residues identical in *Pho* and *Sce* are shown in light blue. The sequence highlighted in the box corresponds to the F_1-β DELSEED region. (C) Domain II (colored pink above the sequences) and previously assigned NHR (Pro122–Pro210 of *Pho* A_1-A subunit, highlighted in the box). Only residues corresponding to Lys117–Pro210 in *Pho* A_1-A subunit are shown. Met189–Pro210 of *Pho* A_1-A subunit and Thr114–Ile136 of bovine F_1-β subunit are homologous (colored gray). Residues identical in all

known sequences of A_1 and V_1-A are shown in blue. Residues identical in *Pho* and *Sce* are shown in light blue. Secondary structure elements including eight β strands of *Pho* Domain II (pink allows represented as S1–S8) and two β strands conserved in Pho and BM (gray allows) are indicated above the sequences.

Table 1 **Crystallographic statistics**

	Native	Se-Met derivative		
		Peak	Edge	Remote
X-ray data				
Wavelength	0.9000	0.9795	0.9797	0.9600
Space group	$P4_32_12$			
Unit cell parameters, *a*, *c* (Å)	128.0, 104.7	128.8, 104.2		
Resolution (Å)[a]	38.6–2.55 (2.64–2.55)	45.2–3.10 (3.27–3.10)	45.2–3.15 (3.32–3.15)	45.2–3.15 (3.32–3.15)
Reflections, observed/ unique	311493/28944	188785/16284	177981/15467	175132/15511
Completeness (%)[a]	99.9 (99.9)	99.9 (99.9)	99.9 (99.9)	99.9 (99.9)
Redundancy[a]	10.8 (11.1)	11.6 (11.8)	11.5 (11.8)	11.3 (11.6)
Averaged I / σ (I)[a]	3.9 (2.0)	7.1 (2.2)	7.4 (2.5)	7.1 (2.4)
R_{meas} (%)[a, b]	11.8 (38.3)	10.5 (37.1)	10.0 (32.0)	10.3 (32.3)
Phasing				
Resolution (Å)		39.5–3.2		
Mean FOM (overall/centric/acentric)		0.72/0.56/0.72		
Refinement				
Resolution (Å)	10.0–2.55			
R/R_{free} (%)	23.9/27.1			
No. of non-hydrogen atoms	4033			
Protein	4025			
MPD	8			
RMSD bond length (Å), angles (°)	0.007, 1.30			
Ramachandran Plot (%)				
Most favored	85.9			
Additionally allowed	11.1			
Generously allowed	3.0			

[a] Values in parentheses are for the outermost resolution shell.

[b] $R_{meas}=\Sigma_h[m/(m-1)]^{1/2}\Sigma_j|<I>_h - I_{h,j}|/\Sigma_h\Sigma_j I_{h,j}$, where $<I>_h$ is the mean intensity of symmetry-equivalent reflections and m is redundancy.

Acknowledgements We would like to thank M. Kawamoto of JASRI and S. Wakatsuki, M. Suzuki, and N. Igarashi of KEK-PF for their assistance in the synchrotron experiments. This work was supported by a grant for the

National Project on Protein Structural and Functional Analyses from the Ministry of Education, Culture, Sports, Science, and Technology of Japan.

References

Abrahams, J. P. & Leslie, A. G. W. (1996). *Acta Cryst.* **D52**, 30-42.

Abrahams, J. P., Leslie, A. G. W., Lutter, R. & Walker, J. E. (1994). *Nature (London)* , **370**, 621-628.

Athappilly, F. K. & Hendrickson, W. A. (1995). *Structure* **3**, 1407-1419.

Becher, B. & Muller, V. (1994). *J Bacteriol*. **176**, 2543-2550.

Berg, A., Vervoort, J. & de Kok, A. (1996). *J Mol Biol*. **261**, 432-442.

Berg, A., Vervoort, J. & de Kok, A. (1997). *Eur J Biochem*. **244**, 352-360.

Bowman, E. J., Tenney, K. & Bowman, B. J. (1988). *J Biol Chem*. **263**, 13994-14001.

Brunger, A. T., Adams, P. D., Clore, G. M., DeLano, W. L., Gros, P., Grosse-Kunstleve, R. W., Jiang, J. S., Kuszewski, J., Nilges, M., Pannu, N. S., Read, R. J., Rice, L. M., Simonson, T. & Warren, G. L. (1998). *Acta Cryst*. **D54**, 905-921.

Collaborative Computational Project, N. (1994). *Acta Cryst.* **D50**, 760-763.

Coskun, U., Chaban, Y. L., Lingl, A., Muller, V., Keegstra, W., Boekema, E. J. & Gruber, G. (2004). *J Biol Chem*. **279**, 38644-38648.

Coskun, U., Radermacher, M., Muller, V., Ruiz, T. & Gruber, G. (2004). *J Biol Chem*. **279**, 22759-22764.

Cowtan, K. (1994). *Joint CCP 4 and ESF-EACBM Newsletter on Protein Crystallography* **31**, 34-38.

Dirmeier, R., Hauska, G. & Stetter, K. O. (2000). *FEBS Letters* **467,** 101-104.

Forgac, M. (1999). *J Biol Chem*. **274,** 12951-12954.

Fortelle, E. d. L. & Bricogne, G. (1997). Vol. 276, *Methods in Enzymology,* pp. 472-494.

Futai, M., Oka, T., Moriyama, Y. & Wada, Y. (1998). *Journal of Biochemistry* **124,** 259-267.

Hara, K. Y., Kato-Yamada, Y., Kikuchi, Y., Hisabori, T. & Yoshida, M. (2001). *J Biol Chem*. **276,** 23969-23973.

Hara, K. Y., Noji, H., Bald, D., Yasuda, R., Kinosita, K. J. & Yoshida, M. (2000). *J Biol Chem***. 275,** 14260-14263.

Hirata, R., Ohsumi, Y., Nakano, A., Kawasaki, H., Suzuki, K. & Anraku, Y. (1990). *J Biol Chem***. 265,** 6726-6733.

Hochstein, L. I. (1992). *FEMS Microbiol Lett*. **97,** 155-159.

Ihara, K. & Mukohata, Y. (1991). *Arch Biochem Biophys*. **286,** 111-116.

Jones, D. D., Stott, K. M., Howard, M. J. & Perham, R. N. (2000). *Biochemistry* **39,** 8448-8459.

Jones, T. A., Zou, J. Y., Cowan, S. W. & Kjeldgaard (1991). *Acta Cryst.* **A47,** 110-119.

Leyva, J. A., Bianchet, M. A. & Amzel, L. M. (2003). *Mol Membr Biol*. **20,** 27-33.

Maegawa, Y., Morita, H., Yao, M., Watanabe, N. & Tanaka, I. (2004). *Acta Cryst*. **D60,** 1484-1486.

Morris, R. J., Perrakis, A. & Lamzin, V. S. (2003). Vol. 374, *Methods Enzymol,* pp. 229-244.

Mukohata, Y. & Yoshida, M. (1987). *J Biochem (Tokyo)*, **101,** 311-318.

Puopolo, K., Kumamoto, C., Adachi, I. & Forgac, M. (1991). *J Biol Chem*. **266,** 24564-24572.

Reddy, D. V., Shenoy, B. C., Carey, P. R. & Sonnichsen, F. D. (2000). *Biochemistry* **39,** 2509-2516.

Schafer, G. & Meyering-Vos, M. (1992). *Biochim Biophys Acta* **1101,** 232-235.

Shao, E. & Forgac, M. (2004). *J Biol Chem*. **279**, 48663-48670.

Shao, E., Nishi, T., Kawasaki-Nishi, S. & Forgac, M. (2003). *J Biol Chem*. **278,** 12985-12991.

Terwilliger, T. (2004). *J Synchrotron Radiat*. **11,** 49-52.

Walker, J. E., Saraste, M., Runswick, M. J. & Gay, N. J. (1982). *EMBO J.* **1,** 945-951.

Wilms, R., Freiberg, C., Wegerle, E., Meier, I., Mayer, F. & Muller, V. (1996). *J Biol Chem*. **271,** 18843-18852.

Yasuda, R., Noji, H., Yoshida, M., Kinosita, K. J. & Itoh, H. (2001). *Nature(London)*, **410,** 898-904.

Zimniak, L., Dittrich, P., Gogarten, J. P., Kibak, H. & Taiz, L. (1988). *J Biol Chem*. **263,** 9102-9112.

Figure 1A

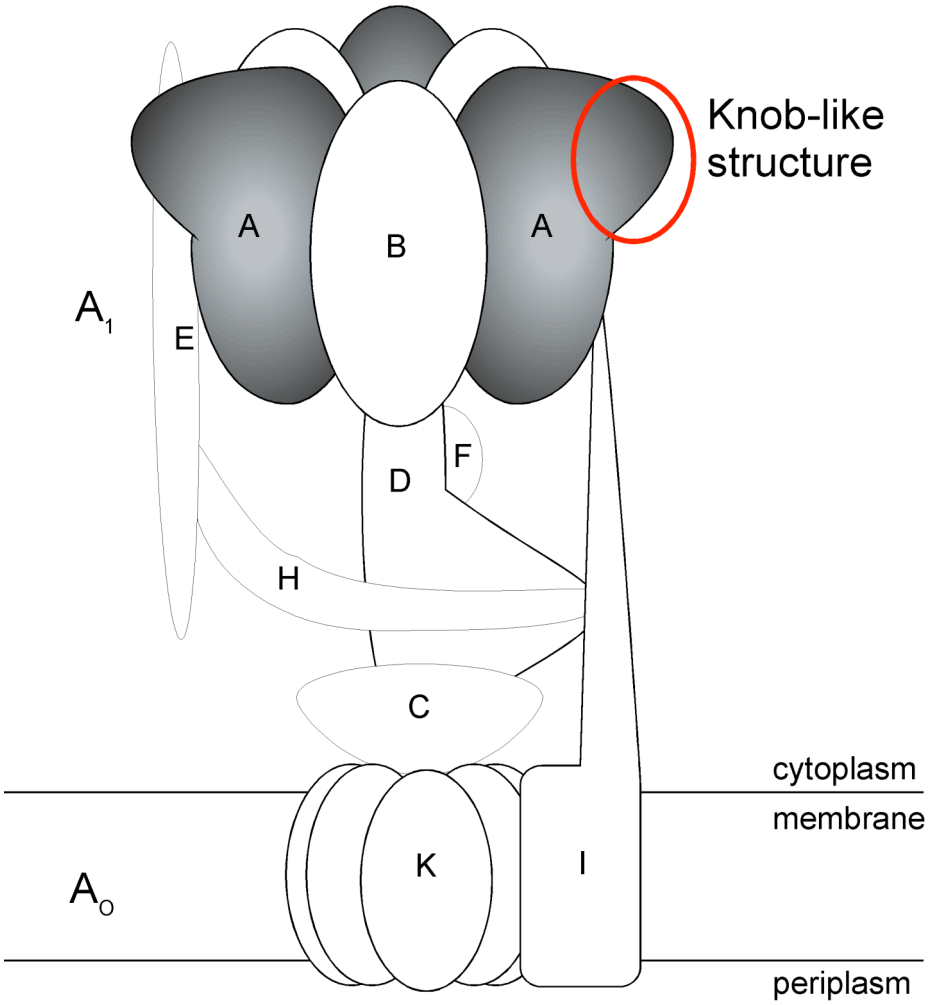
Knob-like
structure
A
B
A
A1
E
F
D
H
C
cytoplasm
membrane
K
I
AO
periplasm

Figure 1B

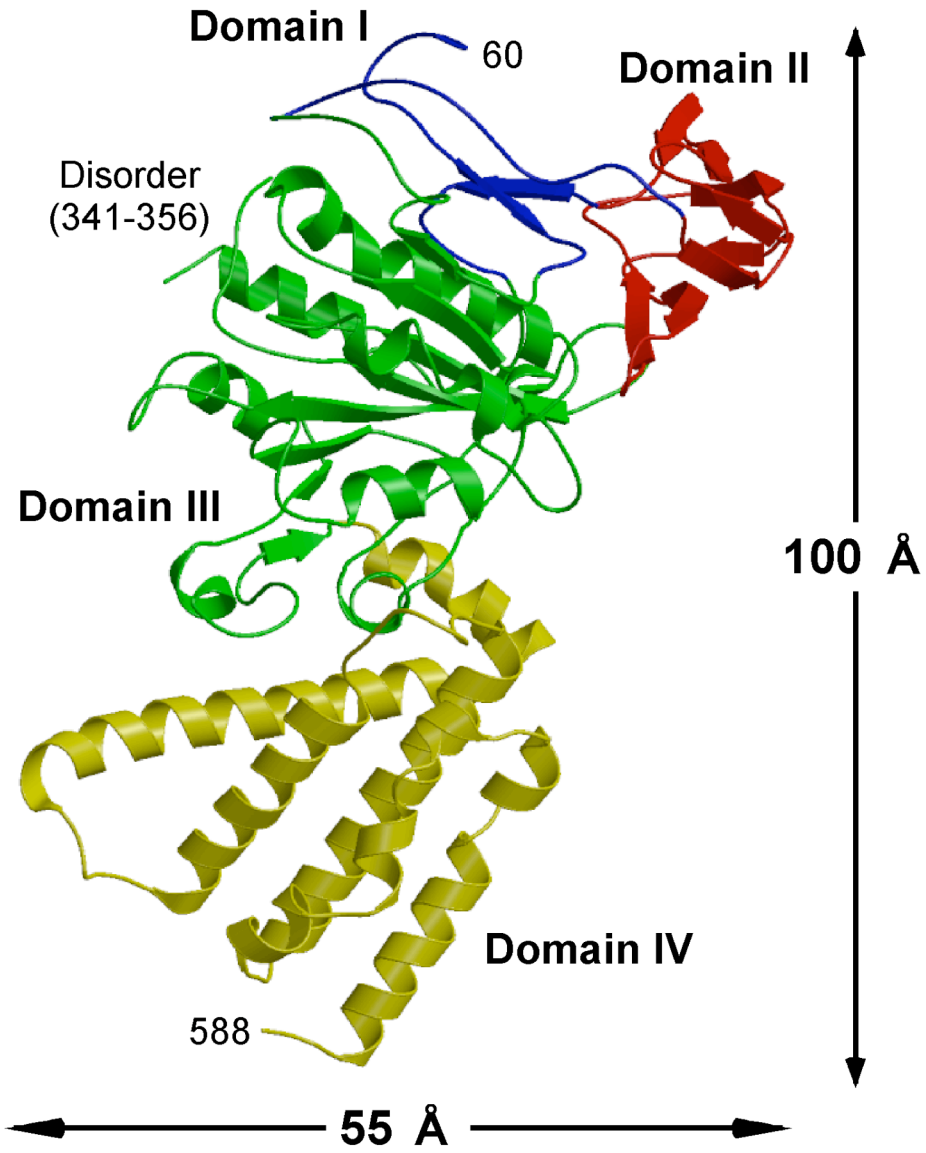
Domain I
60
Domain II
Disorder
(341-356)
Domain III
100 Å
Domain IV
588
55 Å

Figure 1C

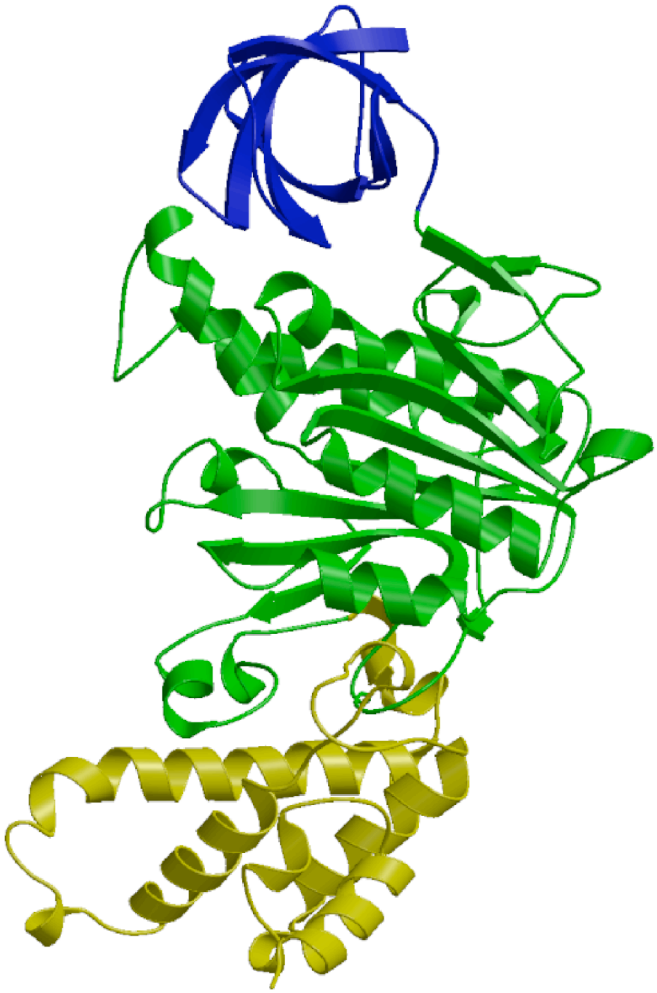

Figure 1D

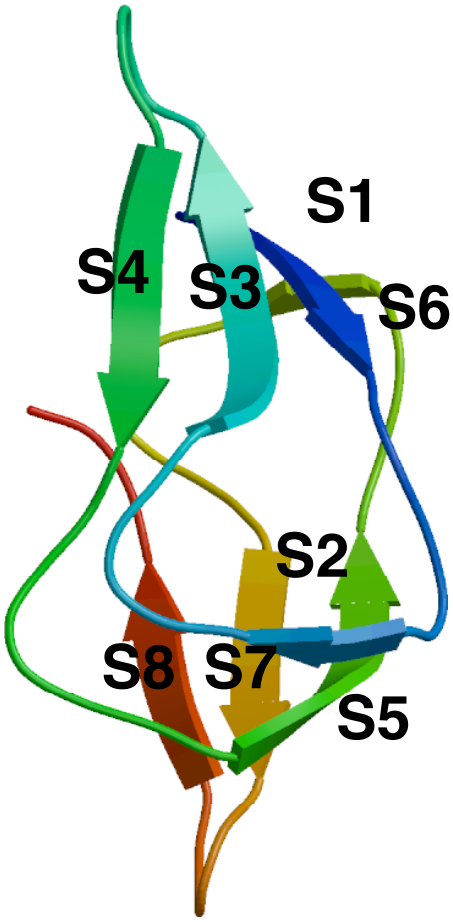

Figure 1E

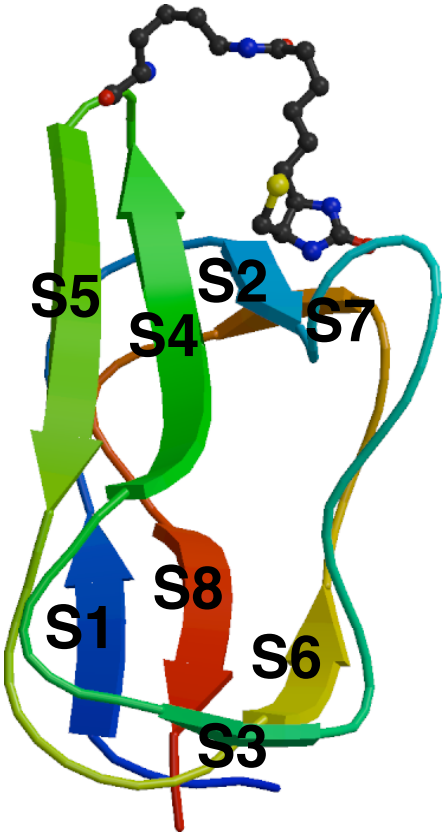

Figure 2A

Figure 2B

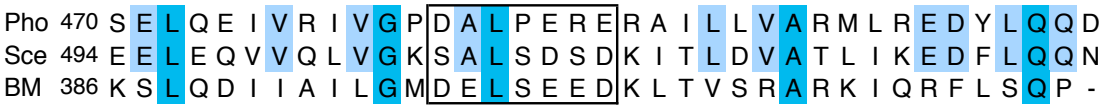

Figure 2C